DEUTSCHES ELEKTRONEN-SYNCHROTRON DESY

DESY 69/23
July 1969

Optical Absorption of Solid Krypton and Xenon in the Far Ultraviolet

R.Haensel, G.Keitel, and P.Schreiber

Physikalisches Staatsinstitut, II. Institut für Experimentalphysik der Universität Hamburg, Hamburg, Germany

and

C. Kunz

Deutsches Elektronen-Synchrotron DESY, Hamburg, Germany

2 HAMBURG 52 · NOTKESTIEG 1

OPTICAL ABSORPTION OF SOLID KRYPTON AND XENON IN THE FAR ULTRAVIOLET*

R. Haensel, G. Keitel, and P. Schreiber
Physikalisches Staatsinstitut, II. Institut für Experimentalphysik der Universität Hamburg, Hamburg, Germany
and
C. Kunz+
Deutsches Elektronen-Synchrotron, Hamburg, Germany

Photoabsorption caused by transitions of the 3d electrons in solid Kr and of the 3d and 4p electrons in solid Xe has been measured. The 7.5-GeV electron synchrotron DESY served as light source. As a comparison the corresponding transitions in the gas have been remeasured. At the onset of d electron transitions, in both solid Kr and solid Xe, absorption line series have been found, which have been identified as "forbidden" excitons in terms of Elliot's theory. At some distance from the onset the broad maximum found earlier in gas absorption and ascribed to the delayed onset of d→f transitions, can also be seen in the solids.

I. INTRODUCTION

Optical measurements on the solid rare gases have been restricted to the fundamental absorption region[1-5] up to 14 eV and to the vicinity of the K edge in Kr and Xe.[6] Electron energy loss measurements have been performed up to 30 eV.[7-10] Apart from these energy ranges no optical experiments have been reported. For the gaseous state however, a large amount of experimental and theoretical material is now available for a wide spectral region. Comparison of optical data of solid rare gases with those in the gaseous state promises new information on the influence of the solid state.

For transitions from the 4d shell in Xe gas Ederer[11] has observed a delayed onset of absorption with a maximum some ten eV above the threshold. This absorption behaviour has theoretically been explained[12-14] as being due to a suppression of the d→f transitions near the threshold which is caused by a centrifugal repulsion potential superimposed on the attractive Coulomb-potential. At a certain distance from the threshold one can expect the atomic behaviour to be a good approximation for the solid state. This has been used for interpretation of the spectra of several metals[14-17] and alkali halides,[18] but to our knowledge no direct experimental comparison of one material in both states of aggregation has been performed to this day. Therefore it seemed especially interesting to compare the continuum absorption of Xe in both the solid and the gaseous state.

Madden and Codling[19] have given a survey of the absorption structures in the rare gases near thresholds for transitions of different types. The corresponding transitions in the solid rare gases should be explainable with the help of energy band calculations and exciton theory. Fowler[20] has performed band calculations for solid Kr and Reilly[21] for solid Xe. Band theory however, only considers one-electron transitions and does not include excitons. Excitons may be described in the two limiting cases of small and large excitons with the help of the Frenkel model and the Wannier model.[22] An intermediate case can be expected[23] for the solid rare gases and Baldini[1] has in fact shown experimentally that excitons in the fundamental absorption region are not only close to the corresponding gas lines (Frenkel picture) but also form line series (Wannier picture).

On the following pages a detailed description of the absorption behaviour of solid Kr due to 3d electron transitions and of solid Xe due to 4d and 4p electron transitions will be given. As a comparison the corresponding transitions have also been investigated in the gaseous state. The Xe 4d transitions near the threshold have already been published in a short letter,[24] but our results of Kr 3d transitions have led to a better understanding of these structures. Details of the experimental arrangement and of the procedure of obtaining the results will be given in Sec. II. In Sec. III the results will be presented and discussed with a view to experiments performed in the fundamental absorption region and to theoretical predictions.

II. EXPERIMENTAL PROCEDURE

A. Light Source and Spectrometer

The measurements have been performed using the 7.5-GeV electron synchrotron DESY as a light source. The spectrum of synchrotron radiation extends continuously from the visible to the x-ray region. In the photon energy region 10 to 500 eV the intensity is much higher than that of conventional (especially continuum) sources. Another advantage, especially for the experiments with samples cooled down to liquid He temperature, is the good vacuum in the synchrotron. More details of the DESY synchrotron radiation may be found elsewhere.[25,26]

The light, concentrated in a narrow cone around the instantaneous flight direction of the electrons, comes through a beam pipe mounted tangentially to the electron orbit in a deflecting magnet. The spectrometer, cryostat, filters etc. are mounted at a distance of 40 m from the tangential point at the accelerator. The experimental arrangement is shown in Fig. 1. The spectrometer used for our measurements is a 1m Rowland mounting. The grazing angle of incidence was: α = 219.6 mrad for the Kr 3d and Xe 4p transitions measurements in the energy range 90 to 160 eV and α = 304.1 mrad for the Xe 4d transition measurements in the energy range 60 to 100 eV. The grating used has a line density of 2400 lines/mm and a blaze angle of $4^{\circ}16'$. The resolution of the instrument as derived from the width of the direct image was approximately 0.1 Å. The energy calibration

was based on gas absorption lines (see Sec. III).

The radiation detector mounted behind the exit slit is an open photomultiplier (Bendix M 306) operated in the D.C. mode. To compensate for fluctuations of the accelerator current the photocurrent from a Cu-Be sheet illuminated by synchrotron light is taken as a monitor signal for the incoming intensity. Both intensity signals are amplified by lock-in amplifiers (Princeton Applied Research, Model HR 8). DESY is operated by a 50 cps repetition rate. Every second pulse of the radiation is suppressed by a chopper wheel mounted in the beam pipe. Thereby the light becomes modulated with 25 cps and noise with 50 cps can be rejected by the tuned amplifiers. The ratio of both signals is formed in the Y-channel of a XY-recorder, whose X-axis is coupled to the wavelength-drive of the spectrometer.

In front of the entrance slit of the spectrometer a concave mirror is mounted, which deflects the beam coming from the accelerator by about 10^{o} and images the source onto the entrance slit. This increases the intensity coming into the spectrometer and reduces background from the high energy part of the synchrotron radiation.

A further reduction of background, caused by light reflected from the grating into higher orders, is achieved by an appropriate angle of incidence to the grating (as mentioned above)

and by using Al filters for the Xe 4d absorption measurements in solid Xe up to 73 eV (the $L_{II,III}$ absorption edge of Al).

B. Absorbing Samples and Data Reduction

For the absorption measurements of the solid rare gases a He cryostat was mounted between the source and the concave mirror. The gas was evaporated onto a 450 Å thick carbon foil cooled down to a temperature just below the sublimation point (40° K for Kr and 55° K for Xe). To avoid contamination the He cooled region was surrounded by a N_2-cooled shield with 40 cm long tubular extensions into both sides of the beam pipe. The pressure in the vacuum system outside the cryostat was kept below 10^{-6} Torr. In this way no evidence of contamination of the carbon foils was found during the measurements (lasting 8 hours on an average). The thicknesses of the solid rare gas films were not measured directly but estimated by comparison with gas absorption (see Sec. III). Typical values ranged between 1000 Å and 10,000 Å. Such films were evaporated in about 1 min.

For the gas absorption measurements the cryostat was replaced by a 7.8 cm long absorption cell with carbon windows on each side.[27] The pressures which were measured by a precision membrane vacuum meter (Datametrics Model 1014) ranged from 2 to 5 Torr for Kr and from 0.1 to 1 Torr for Xe. The accuracy of the instrument is ± 0.1 %, the pressure was kept constant to ± 2 %.

The high purity gas (99.999 %) used in our experiments was of commercial origin (L'Air Liquide). All connections between the absorption cell and the gas reservoir were carefully evacuated to high vacuum before the gas was let into the absorption cell.

The spectra recorded by the XY-recorder were taken with and without absorbers, subsequently digitalized and handled by a computer. Wavelength calibration marks were directly read from a 5 decimal digital voltmeter.

The measurement in the regions of different absorption coefficients have been performed with samples of different thicknesses and with different pressures in the absorption cell in order to check the accuracy of the data as well as to detect and to eliminate higher order straylight. The relative accuracy in the spectral region below 130 eV is about 10 %, in the region above 130 eV the error is increasing continuously up to 25 % since the intensity decreases. Differences in the absorption coefficient in the order of 1 % were clearly detectable if the photon energies were not more than some eV apart.

III. EXPERIMENTAL RESULTS AND DISCUSSION

The absorption curves of Kr from the onset of 3d transitions (90 eV) up to 128 eV are shown in Fig. 2, the curves for 4d and 4p transitions (64 to 155 eV) in Xe are shown in Fig. 3. The overall shape of the spectra - if one disregards the fine structure - is very similar for both gas and solid. This is especially evident for Xe where a broad hump at 100 eV dominates the spectrum. In Kr our energy range was too small to cover the corresponding phenomenon. The onset is almost at the same energy for the gas and the solid. At higher photon energies we find detailed fine structures of different shapes in both states. On the following pages the absorption curves will be discussed in detail.

A. Continuum Absorption

As mentioned in Sec. I. the broad maximum in the absorption of gaseous Xe has for the first time been observed by Ederer[11] and has been explained by Cooper[12] as being caused by the delayed onset of the d→f transitions.

Our results are in excellent agreement with those of Ederer[11] and of Lukirskii et al.[28] whereas they differ somewhat from the calculated cross sections of Cooper[12] and Mc Guire.[29] The same is true for Kr where the experimental agreement with Lukirskii et al.[28] is at 124 eV (= 100 Å) well within the experimental

error, but less in agreement with the theoretical values of Mc. Guire.[29] The absolute error in the σ values of the gases in Figs. 2 and 3 is about ± 10 %. At the higher energy side above 135 eV in Xe the absolute accuracy is only ± 25 % since the intensity in the present adjustments of the spectrometer was too low for these photon energies (see also Sec. II.B.).

Since for the solid Xe and Kr absorption measurements film thickness was not determined the curves in Figs. 2 and 3 have been normalized in such a way that the total absorption integrated over the whole energy range is the same for the solids and the gases. In doing this we find that the curves are in excellent agreement in both states of Kr and Xe before the onset of the d transitions (where still residual absorption structure, due to transitions from the outer shells to high lying states in the continuum, occurs). Moreover their is good agreement in the whole continuum absorption range which is especially striking in Xe where both humps occur at the same photon energy. We have estimated the accuracy with which we are able to prove this overall agreement to be 10 % below 130 eV. Only near the onset of 4p transitions in Xe is the agreement somewhat less, but this may be explained by the reduced absolute accuracy.

B. Excitonic Structure near the Onset of d Transitions

Krypton

Figure 4 shows a detailed view of Fig. 2 near the onset of transitions from the 3d shell of Kr. In the gas curve we see two series of lines caused by the spin orbit splitting of the 3d shell (1.22 eV, see Ref. 30), namely

$$3d^{10}\ 4s^2\ 4p^6\ {}^1S_0 \rightarrow 3d^9\ 4s^2\ 4p^6\ ({}^2D_{5/2})\ np\ {}^1P_1$$

$$(n \geq 5;\ \text{first member } 91.23\ \text{eV})$$

and

$$3d^{10}\ 4s^2\ 4p^6\ {}^1S_0 \rightarrow 3d^9\ 4s^2\ 4p^6\ ({}^2D_{3/2})\ np'\ {}^1P_1$$

$$(n \geq 5;\ \text{first member } 92.45\ \text{eV}).$$

Codling and Madden[30] have given the energy positions of these gas absorption lines on which our energy calibration is based.

In solid Kr a weak peak A can be seen at 90.28 eV followed by many absorption structures. These structures occur in pairs with energy distances of about 1.2 eV, the 3d shell spin orbit splitting energy. The maxima are labeled with unprimed and primed letters. Table I gives the energy positions of the most prominent absorption structures.

Peaks B, C and B', C' are of special interest. They are especially sharp, the width being comparable to that of the gas absorption lines. B and B' are very close to the first members of the gas absorption lines but their oscillator strengths being much smaller. In analogy to the situation in the fundamental absorption region[1] we believe that B, C and B', C' are members of a Wannier exciton series.

Besides those excitons which are responsible for the structure in the fundamental absorption region[1] and which are formed at band singularities between which optical interband transitions are allowed, there can exist, according to Elliot,[31] a second class of excitons ("forbidden" excitons) at critical points, where optical interband transitions are forbidden. These excitons also show hydrogen-like Rydberg series of absorption lines but n=1 is missing. According to Fowler's band calculation[20] the lowest point of the conduction band in solid Kr is the s-symmetric Γ_1 point. Since the lowest point with odd symmetry accessible for first class excitons can only be found several eV above the bottom of the conduction band, we believe that B, B' and C, C' are the n=2 and n=3 members of a second class exciton series coupled to Γ_1.

According to a Rydberg formula the Wannier series form hydrogen-like series such as

$$E = E_o - \frac{E_b}{n^2} \text{ with } E_b = \frac{e^4 \mu}{2\hbar^2 \epsilon^2} , \qquad (1)$$

where E is the exciton energy, E_o is the series' limit, E_b is the exciton binding energy, μ is the reduced exciton mass and ε the dielectric constant. The binding energy E_b for a second class series is found to be 2.7 eV for the first series (B, C) and 2.3 eV for the second (B', C'); consequently E_o is 92.3 eV and 93.5 eV. The binding energies for the corresponding first class valence band excitons are according to Baldini[1] 1.7 eV and 1.5 eV. The higher values for the core exciton binding energies are intelligible due to the higher effective mass μ. Were the peaks B and C to be n=1 and n=2 members of a first class exciton series, then the calculation of E_b would give only 0.5 eV and 0.4 eV which would be unreasonably low.

Thus also peak A would now be understandable as being the theoretically forbidden n=1 member, which is not completely suppressed, due perhaps to crystal imperfections in the solid Kr film. Its energy position at 90.28 eV is not exactly what it should be if calculated according to Eq. (1) (namely 89.56 eV), but such a deviation is usually the case for the n=1 exciton.[1]

Another support for the assumption of a second order exciton series comes from the comparison of the oscillator strengths in B, B' and C, C'. Their ratio is much closer to 2.6 : 1 evaluated[31] for n=2/n=3 of a second class exciton series, than to 8 : 1 evaluated for n=1/n=2 of a first class exciton series.

Xenon

These conclusion lead to the assumption that a similar situation occurs near the threshold of the 4d transitions in Xe. Fig. 5 shows a detailed view of the low energy region in Fig. 3 (preliminary results have been published before[24]).

In the gas curve two line series, namely

$$4d^{10}\ 5s^2\ 5p^6\ {}^1S_0 \rightarrow 4d^9\ 5s^2\ 5p^6\ ({}^2D_{5/2})\ np\ {}^1P_1$$

$$(n \geq 6;\ \text{first member } 65.09\ \text{eV})$$

and

$$4d^{10}\ 5s^2\ 5p^6\ {}^1S_0 \rightarrow 4d^9\ 5s^2\ 5p^6\ ({}^2D_{3/2})\ np'\ {}^1P_1$$

$$(n \geq 6;\ \text{first member } 67.02\ \text{eV})$$

can be seen, converging at 67.55 eV and 69.52 eV, thus giving a spin orbit splitting energy for the 4d shell of 1.97 eV.[30]

In solid Xe, in accordance with Kr, B, B' and C, C' are also assumed to be the first members of a second class series. The structure C is not as clear as in solid Kr and therefore E_b = 1.4 eV and E_b' = 2.1 eV as well as E_o = 65.6 eV and E_o' = 67.8 eV are not so well established. Again peak A would be the not completely suppressed n=1 exciton. According to Reilly's band calculation[21] which are very similar to those of solid Kr the bottom of the conduction band has even parity and the first odd parity states are at 5 eV higher energies.

Other Discrete Structures

Beyond the first excitons in solid Kr and Xe other discrete structures are to be seen in Figs. 2-5. They may be metastable excitons or van Hove singularities in interband transitions. An assignement to specific singularities in the conduction band, however, is impossible at the present time.

In the gas absorption curves of Figs. 2 and 3 some structures can be found for Kr near 110 eV and for Xe near 80 eV, which have previously been observed by Codling and Madden,[32] who ascribed these to double excitation of electrons in the d and in the outer p shell. In the same region the absorption curves of solid Kr and Xe also show specific structures which are especially evident in solid Xe. As in the case of the gas their oscillator strengths are much weaker than that of the single d electron transitions.

In this connection it should be noted that Hermanson[33] made an estimation of double quantum excitation probability on alkali halides with the result that it should be weaker by two orders of magnitude than that of single quantum excitations. This is in contrast to Miyakawa[34] who stated that both types of excitations should occur with similar probability. Our present results together with recent photoemission data[35] are in favour of Hermanson's theory.

The onset of transitions from the 4p shell in Xe around 140 eV can be seen in the inset of Fig. 3. The gas structure has already been investigated by Codling and Madden.[32] In agreement with our own results for gaseous Xe the authors only find evidence of transitions from the 4p (3/2) shell. They ascribe the absence of structures from 4p (1/2) shell transitions to the fact that these contributions are deep in the 4p (3/2) continuum since the spin-orbit splitting energy of 4p is expected to be relatively large (about 8 eV). This should substantially decrease the lifetime of discrete states formed by transitions from the 4p (1/2) shell. It is therefore very surprising that in solid Xe at about 150 eV two peaks can be seen similar to those at 142 eV. They are obviously due to transitions from the 4p (1/2) shell.

ACKNOWLEDGMENTS

The authors are grateful to the directors of the Deutsches Elektronen-Synchrotron and the Physikalisches Staatsinstitut, particularly to Prof. P. Stähelin, for continuous interest in this work and for valuable support of the synchrotron radiation group. Thanks are also due to H. Dietrich, M. Lehnert, D. Michael, G. Singmann, and E.-W. Weiner for technical assistance during the course of experiments. Stimulating discussions on the subject with Drs. G. Baldini, J.J. Hopfield, D.W. Lynch, Y. Onodera, and B. Sonntag and comments by Drs. R.P. Madden and M.H. Reilly are gratefully acknowledged.

≠ Work supported in part by the Deutsche Forschungsgemeinschaft

+ Present address: Department of Physics and Astronomy, University of Maryland, College Park, Md. 20742

1. G. Baldini, Phys.Rev. 128, 1562 (1962)
2. O. Schnepp and K. Dressler, J.Chem.Phys. 33, 49 (1960)
3. I.T. Steinberger and O. Schnepp, Sol.State. Comm. 5, 417 (1967)
4. D. Beaglehole, Phys.Rev. Letters 15, 551 (1965)
5. J.F. O'Brien and K.J. Teegarden, Phys.Rev. Letters 17, 919 (1966)
6. J.A. Soules and C.H. Shaw, Phys.Rev. 113, 470 (1959)
7. E.M. Hörl and J.A. Suddeth, J.Appl.Phys. 32, 2521 (1961)
8. H. Boersch, O. Bostanjoglo, and L. Schmidt, Tagung für Elektronenmikroskopie, Aachen 1965 (unpublished)
9. P. Keil, Z. Naturf. 21a, 503 (1966)
10. P. Keil, Z. Phys. 214, 251 (1968)
11. D.L. Ederer, Phys.Rev. Letters 13, 760 (1964)
12. J.W. Cooper, Phys.Rev. Letters 13, 762 (1964)
13. S.T. Manson and J.W. Cooper, Phys.Rev. 165, 126 (1968)
14. U. Fàno and J.W. Cooper, Rev.Mod.Phys. 40, 441 (1968)
15. R. Haensel, C. Kunz, T. Sasaki, and B. Sonntag, Appl.Opt. 7, 301 (1968)
16. B. Sonntag, R. Haensel, and C. Kunz, Sol.State Comm. 7, 597 (1969)
17. P. Jaeglé and G. Missoni, Compt. Rend. 262, 71 (1966)
18. H. Fujita, C. Gähwiller, and F.C. Brown, Phys.Rev. Letters 22, 1369 (1969)

19. R.P. Madden and K. Codling, in Autoionization; Astrophysical, Theoretical, and Laboratory Experimental Aspects, edited by A. Temkin (Mono Book Corporation, Baltimore, Md., 166), p. 129.
20. W.B. Fowler, Phys.Rev. 132, 1591 (1963)
21. M.H. Reilly, J.Phys.Chem. Solids 28, 2067 (1967)
22. R.S. Knox, The Theory of Excitons (Academic Press, New York and London, 1963)
23. Y. Toyozawa, M. Inoue, T. Inui, M. Okazaki, and E. Hanamura, J.Phys.Soc. Japan 22, 1337 (1967)
24. R. Haensel, G. Keitel, P. Schreiber, and C. Kunz, Phys.Rev. Letters 22, 398 (1969)
25. R. Haensel and C. Kunz, Z. Angew. Physik 37, 276 (1966)
26. R.P. Godwin, in Springer Tracts in Modern Physics, Vol. 51, edited by G. Höhler (Springer Verlag Berlin, Heidelberg, New York, 1969) (to be published)
27. H. Wöhl, Diplomarbeit, Universität Hamburg, 1968 (unpublished)
28. A.P. Lukirskii, I.A. Brytov, and T.M. Zimkina, Opt. i. Spectroscopiya 17, 438 (1964) (English transl.: Opt. Spectry. (USSR) 17, 234 (1964)
29. E.J. Mc Guire, Phys.Rev. 175, 20 (1968)
30. K. Codling and R.P. Madden, Phys.Rev. Letters 12, 106 (1964)
31. R.J. Elliot, Phys.Rev. 108, 1384 (1957)
32. K. Codling and R.P. Madden, Appl.Opt. 4, 1431 (1965)
33. J.C. Hermanson, Phys.Rev. 177, 1234 (1969)
34. T. Miyakawa, J.Phys.Soc. Japan 17, 1898 (1962)
35. R. Haensel, G. Keitel, C. Kunz,G. Peters, P. Schreiber, and B. Sonntag, to be published

Figure captions:

Fig. 1 Experimental arrangement. EO = electron orbit, V = valve, Sh = shielding, BS = beam shutter, CW = chopper wheel, Mo = monitor (Cu-Be sheet), F = filter, C = cryostat, M = mirror, ES = entrance slit of the Rowland monochromator, RA = rotating arm, G = grating, D = detector (photomultiplier behind the exit slit)

Fig. 2 Cross section versus photon energy for solid (solid curve) and gaseous (dashed curve) krypton in the energy range 90 - 128 eV. The cross section for gaseous krypton is given absolutely in megabarns (10^{-18} cm^2) with an error of 10 %. The curve for solid krypton is adjusted in such a way, that the integrated oscillator strengths become equal for both solid and gaseous krypton.

Fig. 3 Cross section versus photon energy for solid (solid curve) and gaseous (dashed curve) xenon in the energy range 64 - 155 eV. The cross section for gaseous xenon is given absolutely in megabarns (10^{-18} cm^2) with an error of 10 %. The curve for solid xenon is adjusted in such a way, that the integrated oscillator strengths become equal for both solid and gaseous xenon. The inset shows the cross sections in the region of 4p electron excitation in an extended scale.

Fig. 4 Cross section versus photon energy for solid (solid curve) and gaseous (dashed curve) krypton near the onset of 3d electron excitation. The cross section for the solid has been multiplied by a factor of two. In the gas the members of the two spin-orbit splitted line series $3d^{10}\ 4s^2\ 4p^6\ {}^1S_o \rightarrow 3d^9\ 4s^2\ 4p^6\ ({}^2D_{5/2})\ np\ {}^1P_1$ and $3d^{10}\ 4s^2\ 4p^6\ {}^1S_o \rightarrow 3d^9\ 4s^2\ 4p^6\ ({}^2D_{3/2})\ np'\ {}^1P_1$ are denoted by np and np' resp. In the solid the most important structures are labeled with capital letters, unprimed and primed letters showing up spin-orbit pairs.

Fig. 5 Cross section versus photon energy for solid (solid curve) and gaseous (dashed curve) xenon near the onset of 4d electron excitation. The cross section for the solid has been multiplied by a factor of two. In the gas the members of the two spin-orbit splitted line series $4d^{10}\ 5s^2\ 5p^6\ {}^1S_o \rightarrow 4d^9\ 5s^2\ 5p^6\ ({}^2D_{5/2})\ np\ {}^1P_1$ and $4d^{10}\ 5s^2\ 5p^6\ {}^1S_o \rightarrow 4d^9\ 5s^2\ 5p^6\ ({}^2D_{3/2})\ np'\ {}^1P_1$ are denoted by np and np' resp. In the solid the most important structures are labeled with capital letters, unprimed and primed letters showing up spin-orbit pairs.

Table I. Energy positions of the most prominent structures in solid Xe and solid Kr.

Structure	Energy (eV)	
	Solid Xe	Solid Kr
A	64.36 ± 0.08	90.28 ± 0.08
B	65.28 ± 0.04	91.61 ± 0.04
B'	67.24 ± 0.04	92.90 ± 0.04
C	65.48 ± 0.05	91.99 ± 0.04
C'	67.53 ± 0.1	93.22 ± 0.04
D	65.87 ± 0.08	92.13 ± 0.05
D'	67.87 ± 0.05	
E	66.60 ± 0.08	94.19 ± 0.05
E'		95.34 ± 0.08
F	66.79 ± 0.05	94.62 ± 0.08
F'	68.68 ± 0.05	
G	69.98 ± 0.05	94.96 ± 0.05
G'		96.28 ± 0.1
H	72.17 ± 0.07	95.82 ± 0.06
H'	74.19 ± 0.07	96.97 ± 0.06
I		98.18 ± 0.06
I'		99.47 ± 0.06
J		98.75 ± 0.06
J'		
K		101.05 ± 0.06
K'		102.33 ± 0.06

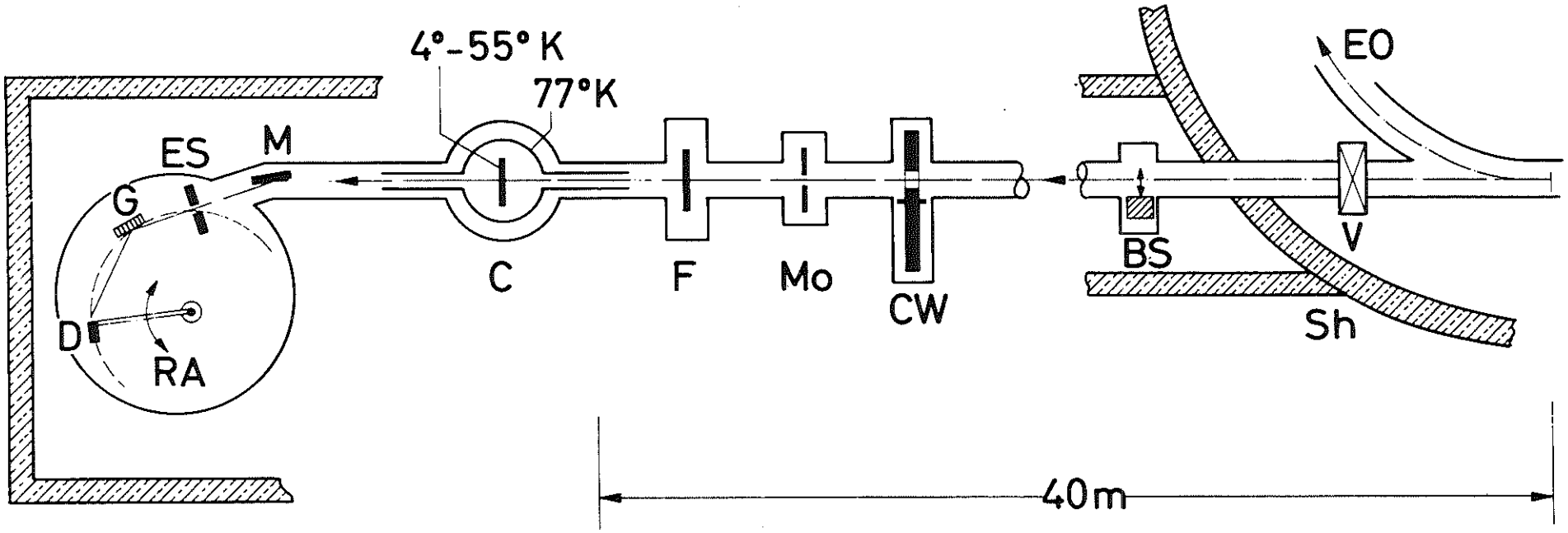

Fig. 1

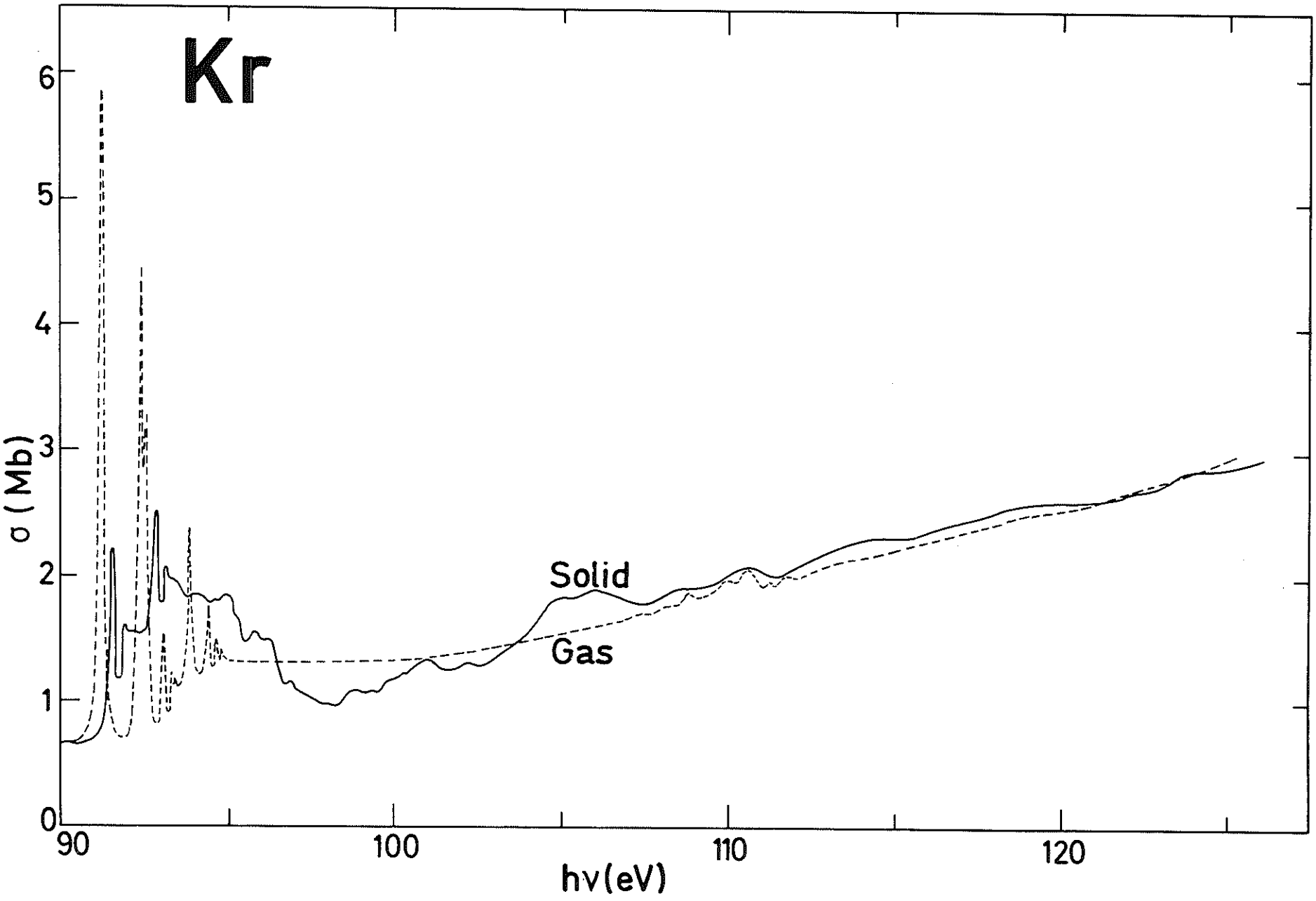

Fig. 2

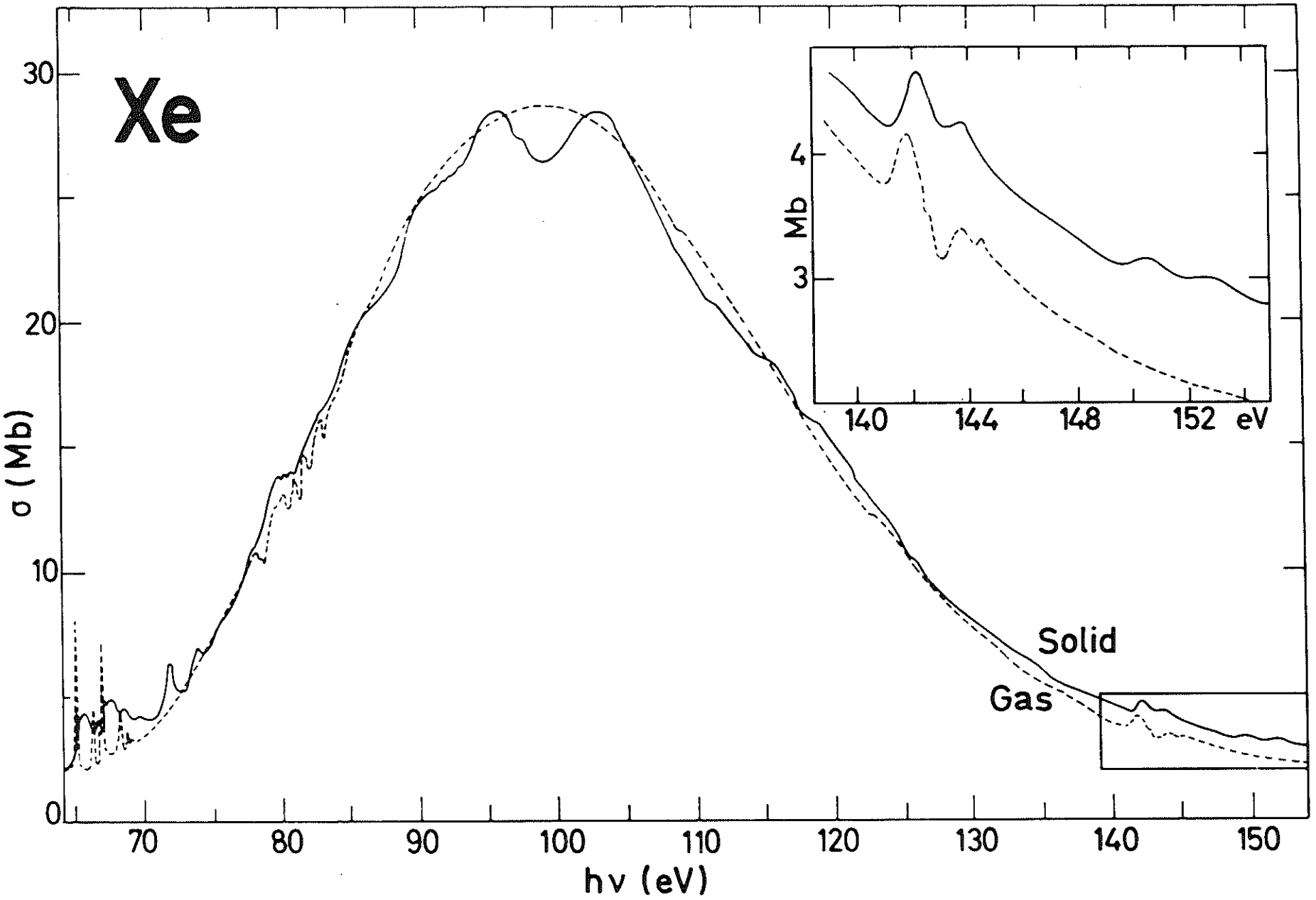

Fig. 3

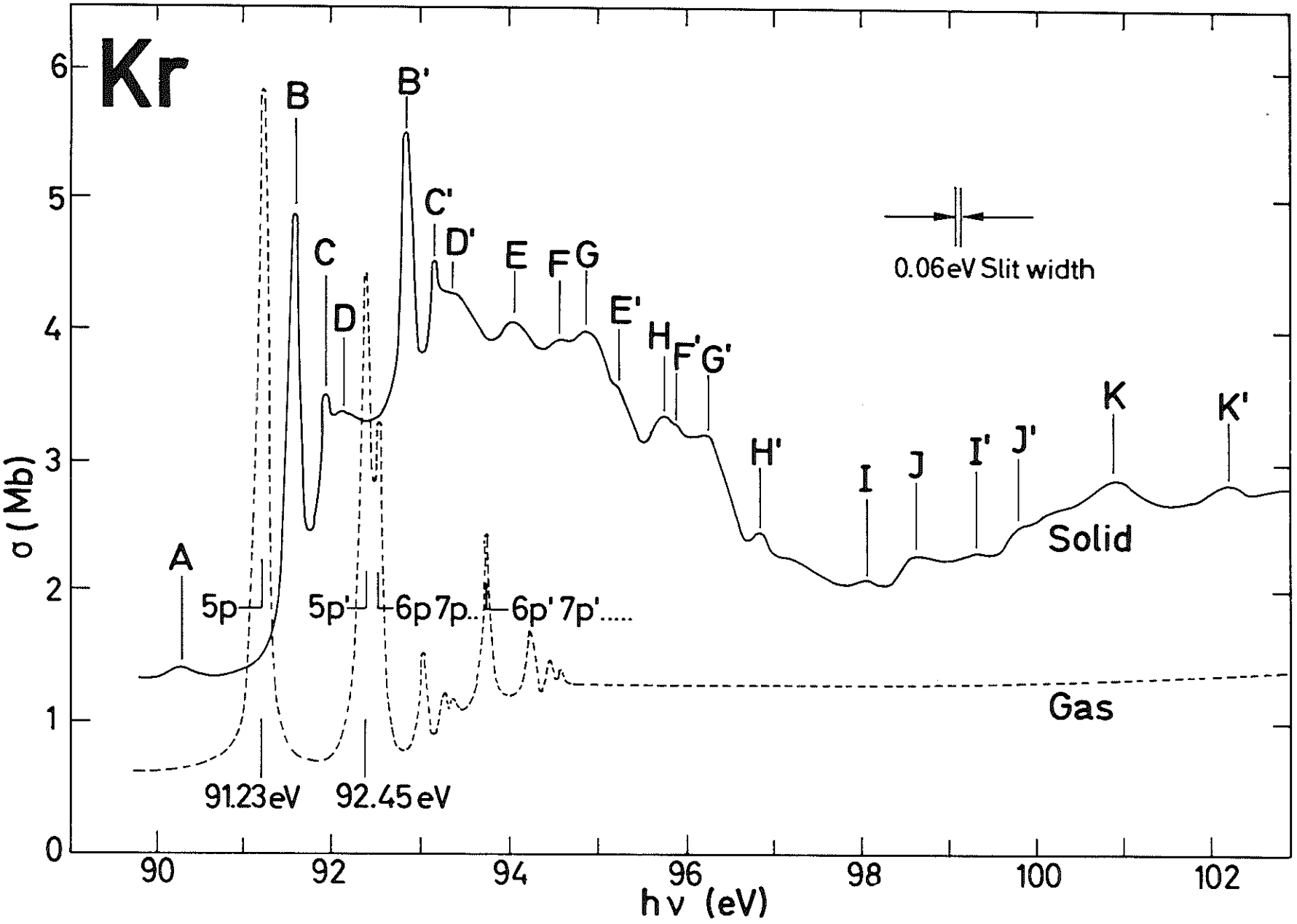
Kr
σ (Mb)
hν (eV)
A
B
B'
C
C'
D
D'
E
F
G
E'
H
F'
G'
H'
I
J
I'
J'
K
K'
5p
5p'
6p 7p...
6p' 7p'.....
91.23eV
92.45eV
0.06eV Slit width
Solid
Gas

Fig. 4

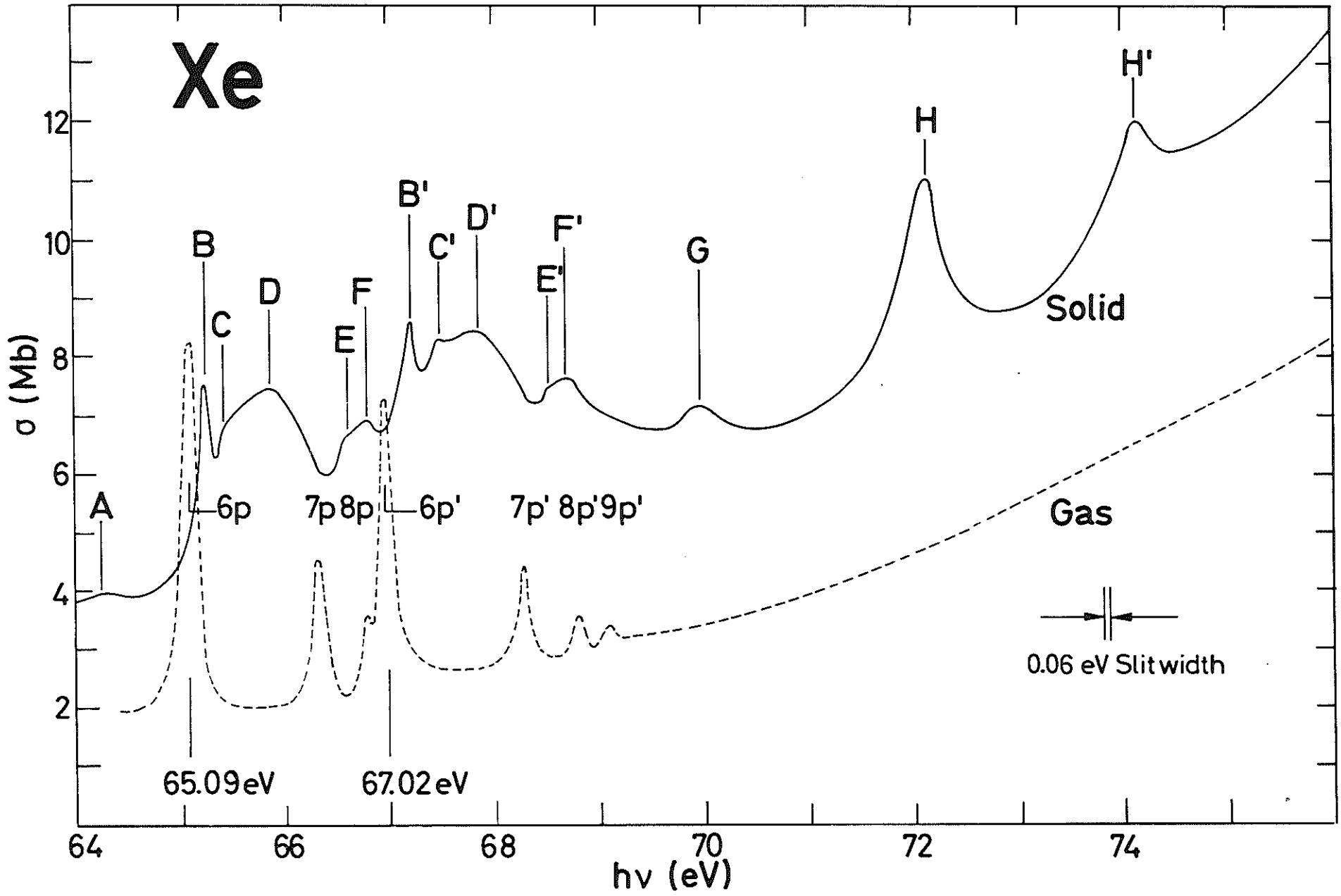
Xe
σ (Mb)
hν (eV)
A
B
C
D
E
F
B'
C'
D'
E'
F'
G
H
H'
6p
7p 8p
6p'
7p' 8p' 9p'
Solid
Gas
0.06 eV Slit width
65.09 eV
67.02 eV
2
4
6
8
10
12
64
66
68
70
72
74

Fig. 5